Algethami et al., J Nanomater Mol Nanotechnol 2017, 6:4
DOI: 10.4172/2324-8777.1000222

Journal of Nanomaterials & Molecular Nanotechnology

Research Article

A SCITECHNOL JOURNAL

Bismuth Sulfide Nanoparticles as a Complement to Traditional Iodinated Contrast Agents at Various X-Ray Computed Tomography Tube Potentials

Merfat Algethami[1], Anton Blencowe[2,3], Bryce Feltis[4] and Moshi Geso[1*]

Abstract

Background: Investigation of the contrast enhancement effects on the CT images of the conventional iodinated contrast media (CM) or bismuth sulfide nanoparticles (Bi_2S_3 NPs) with increasing x-ray tube potentials.

Materials and methods: A phantom was filled with iodinated CM or Bi_2S_3 NP solutions at concentrations ranging from 0 to 65 mM and the phantom was scanned with a CT scanner using tube potentials of 80, 100, 120 and 140 kVp at a fixed current of 200 mA. The CT contrast enhancement and contrast-to-noise ratios (CNR) of all scanned images were calculated.

Results: This study demonstrated that greater image contrast was observed with Bi_2S_3 NPs compared to the iodinated CM at all concentrations and energies (80-140 kVp) tested. For example, at a concentration of 65 mM and tube potential of 140 kVp, a CNR enhancement of three to four times was observed for Bi_2S_3 NPs compared to iodinated CM. Even at a conventional tube potential of 80 KVp, one to two-fold increase in CNR was noted for Bi_2S_3 NPs. Results are also demonstrated that CNR increased with increasing concentration of Bi_2S_3 NPs at a fixed tube potential.

Conclusion: These results highlight the effects of the different physical densities and atomic numbers of the two elements (I versus Bi), and their role in enhancing the probability of Compton scattering (CS) and photoelectric effects (PEs). As tube potential was increased, the CT numbers for both Bi_2S_3 NPs and iodinated CM decreased, consistent with a decrease in the probability of CS and PEs with increasing beam energy. However, the rate of decrease for iodinated CM was larger than Bi_2S_3 NPs. A good correlation was observed between the experimental results and the theoretical spectra based on linear attenuation coefficients.

Keywords

Bi_2S_3; Nanoparticles; Contrast agent; Computed tomography; Contrast medium

Introduction

Medical imaging modalities, such as magnetic resonance imaging (MRI), computed tomography (CT), positron emission topography (PET) and single photon emission computed tomography (SPECT) are commonly used to diagnose and guide treatment. X-ray CT is the most frequently employed, owing to its availability, low cost, deep tissue penetration, and ability to provide high-resolution 3D images of anatomical structures in a short timeframe. However, while CT can generate highly detailed tomographic images of electron-dense materials, its ability to differentiate subtle changes between soft tissues is limited. This is because most soft tissues have very similar CT numbers, ranging from -100 to 100 Hounsfield units (HU), which are a measure of X-ray attenuation in CT images [1,2]. Consequently, CT contrast agents with high X-ray attenuation coefficients are necessary for contrast enhancement in regions of interest [3].

The interaction between the incident radiation and the contrast media results in significant contrast improvements for diagnostic imaging of soft tissues. Contrast agents based on iodinated compounds have been used extensively in radiologic imaging since the 1920s [4-7]. Despite effective attenuation, versatile synthesis methods, high solubility and body tissue tolerance, iodinated contrast agents suffer from several drawbacks, especially for certain groups of patients [4,8-10]. The main limitation of iodinated contrast agents is their short circulation times (<10 min) resulting from renal clearance by the kidneys, and thus rapid CT image acquisition is required [11,12]. In addition, iodinated contrast agents have a non-specific bio-distribution throughout the intravascular and extravascular spaces resulting in poor contrast, especially in larger patients [4,13,14]. Generally, larger doses of contrast agents are required to counteract their rapid renal elimination, which can induce hypersensitivity reactions and can have other serious adverse effects [15-17].

Recently, several strategies have been introduced to improve the efficiency and reduce the toxicity of iodinated contrast agents. For example, polymeric and lipid nanoparticulate systems have been used to encapsulate iodinated contrast agents [4,14,18,19]. However, these approaches have had limited success due to the high concentrations of iodinated contrast agents required for encapsulation and lengthy purification methods [20]. Furthermore, targeted imaging with these nanoparticulate systems still remains a major challenge due to the difficulty in conjugating specifically targeted biological components to these materials and the subsequently low payloads/concentrations that are delivered to the target, resulting in low CT sensitivity [6,21].

In CT scans, the majority of photons used at the image receptor are of high energy (>60 KeV). However, the atomic number (Z=53) and K-edge value (33.2 KeV) of iodine means that its contrast is only sensitive to low energy X-rays. This is due to the high absorption of low-energy photons, which results in a beam-hardening artefact. In other words, the low energy photons that are absorbed have less contribution in the CT diagnostic energy range. The result of this is that iodine has its optimal effect only at low energy. Thus, higher atomic number elements are more desirable to enhance the CT efficiency.

The development of various nanoscale metal-based contrast agents has been proposed as a means to overcome the shortcomings of traditional iodinated contrast agents [4,22]. In particular, nanoparticle (NP)-based contrast media deliver heavy atoms with greater bio-

***Corresponding author:** Moshi Geso, Discipline of Medical Radiations, School of Health and Biomedical sciences, RMIT University, Melbourne, Victoria 3109, Australia, Tel: +61399257991; E-mail: moshi.geso@rmit.edu.au

Received: May 02, 2017 **Accepted:** June 02, 2017 **Published:** June 07, 2017

compatibility, higher contrast densities and longer circulation times to targets more efficiently than conventional contrast agents [23]. These longer circulation times facilitate the imaging process and allow better visualization of blood vessels and tumours. Recently, high density metals such as gold (Au) and bismuth (Bi) have been formulated as nanoparticles and have been shown to have relatively long blood circulation times compared to iodinated contrast agents.

Au NPs with diameters of 1.9 nm have been reported to have circulation times of ~ 15 h in mice [24], whereas bismuth sulfide (Bi_2S_3)-NPs (50 nm) have demonstrated that the circulation times of 140 min [12], both significant improvements on clinical iodinated contrast agents (<10 min).

There have also been numerous advances in the preparation of Au NPs as contrast agents for CT, with their size, shape and surface coating being tunable parameters [25-28]. However, the widespread use of Au remains low due the high costs involved.

Bismuth is low toxic, cost effective alternatives to Au. Bismuth-based compounds have also been used for many years for the treatment of various conditions and diseases. For example, bismuth containing pharmaceuticals are used for the treatment of gastrointestinal disorders [29-31], such as the eradication of Helicobacter pylori in peptic ulcers [29,32-34], syphilis, tumours [35] and for reducing the renal toxicity caused by cisplatin [36]. Bismuth-based NP contrast agents for CT possess several advantages over conventional iodinated and Au-based NP contrast agents as a result of their high atomic number (Z=53 (I); 79 (Au); 83 (Bi)), high X-ray attenuation [12,20,37,38], low cost (~$ 0.02 g^{-1}) [20,37,39], and low toxicity [12,40]. Bi_2S_3 is one of the most promising NP contrast agents due to its high effective nuclear charge (Zeff=76.2), physical density (ρm=6780 $Kg.m^{-3}$), and electron density (ρe=2.20×1029 $e.m^{-3}$). This high density of free electrons increases the probability for Compton scattering, which is of particular interest in X-ray-based imaging and radiotherapy [4].

Rabin et al. demonstrated that polyvinylpyrrolidone (PVP) coated Bi_2S_3 NPs displayed a five-fold increase in CT signal enhancement at a tube potential of ~50 KVp and a lower-cytotoxicity profile compared to the iodine contrast agent Iopromide in liver hepatocyte (HepG2) cells and similar cytotoxicity profiles were also reported in macrophage (U937) cells [12]. Cytotoxicity studies comparing Bi_2S_3 NPs and Bi subsalicylate in these cell lines demonstrated higher cytocompatibility with the former. Kinsella et al. conjugated Bi_2S_3 NPs with Lyp-1 cyclic peptides, a specific target for breast cancer in mice [41]. Following intravenous administration and CT scanning, the conjugated Bi_2S_3 NPs were found to produce clearer images and higher CT numbers in the target tumours compared to non-targeted NPs [41]. In addition to diagnostic applications, there has been recent interest in the use of Bi_2S_3 NPs as radiosensitisers for cancer therapy. In both phantom [42] and cell studies [40], we have demonstrated that Bi_2S_3NPs were superior to Au NP for radiation dose enhancement.

In this study, we aimed to validate our previous work and demonstrate that Bi_2S_3 NPs provide significant increases in X-ray attenuation rates at clinical tube potentials ranging from 80 to 140 KVp, in comparison to conventional iodinated contrast agents. This work highlights the potential of Bi_2S_3 NPs to provide higher contrast and more detailed CT images.

Experimental

Materials and syntheses

Materials: Oleic acid (99.9%), oleyl amine (70%), octadecane (99%), thioacetamide (99%) and bismuth neodecanoate were purchased from Sigma Aldrich, United States. Poly (vinyl pyrrolidone) (MW=8000) was purchased from Alfa Aesar, United States. Omnipaque™ (Iohexol; 350 mg/mL) was purchased from GE Healthcare, United Kingdom. All chemicals were used without further purification unless otherwise stated. PVP coated Bi_2S_3 NPs with diameters of 5-15 nm were synthesized as reported previously [37,40].

Preparation of Bi2S3 NP solutions: Bi_2S_3 NPs (56.6 mg) were suspended in Milli-Q water (2.2 mL) with sonication (100 W) for 10 min. The resulting stock solution was diluted with Milli-Q water to obtain solutions with Bi concentrations ranging from 0 to 65 mM.

Preparation of iodine solutions: Clinical iodinated contrast media (Omnipaque 350 mgI.mL-1) was utilized for comparison in this study. The Omnipaque stock was diluted with Milli-Q water to afford solutions with iodine concentrations ranging from 0 to 65 mM.

Characterization

Dynamic light scattering (DLS) was conducted on a Malvern Zetasizer Nano ZS 90, and was employed to determine the hydrodynamic diameter (Dh) of Bi_2S_3 NPs. Transmission electron microscopy (TEM) was used to observe the morphology and size of the Bi_2S_3 NPs. TEM images were acquired using a JEOL TEM 1010 with an accelerating voltage of 100 KeV. Samples were prepared by evaporating the dilute solutions of NPs in isopropyl alcohol (IPA) onto strong carbon-coated copper grids and air drying before TEM. X-ray powder diffraction (XRD) spectroscopy was carried out using an X-ray diffractometer (D8 ADVANCE, Bruker AXS) with a Cu-Ka radiation source.

CT scanning

CT images were acquired using a Light Speed™ VCT scanner (single-slice) (GE Healthcare, Waukesha, WI, USA) at the Heidelberg Repatriation Hospital, Australia. Samples were imaged in Perspex phantoms positioned at the iso-center of the CT gentry. Phantoms consisted of eight holes filled with Omnipaque and Bi_2S_3 NPs solutions (2 mL) at concentrations ranging from 0 to 65 mM (Figure 1). The phantom consisted of five blocks in parallel to mimic 5 cm^2 of equivalent attenuation. CT imaging was initially conducted at a tube potential of 80 kVp and current of 200 mA, with a slice thickness of 5 mm. Subsequently, CT scanning was repeated at tube potentials of 100, 120 and 140 KVp whilst keeping all other parameters constant. The CT value, in Hounsfield Units (HU) for each sample and tube potential was determined from three different slices (the top, middle and bottom slices) and then averaged.

Contrast-to-noise ratio (CNR)

The CNR (background Perspex to contrast agents) was selected as a standardization method to compare the two contrast agents. The region of interest (ROI) in each sample image was drawn around with a 4 mm diameter circle. The mean in pixels of each ROI in each sample and the mean of the background area of the phantom were calculated. The CNR is expressed as [43]:

$$CNR = \frac{ROI_m - ROI_b}{SD_b}$$

The ROIm and ROIb represent the CT values of the contrast material in a ROI of the samples and in the background of phantom, respectively. SDb represents the standard deviation of the CT number of the background. CNR values were collected for both contrast agents at each tube potential and evaluated for differences in the mean using one tail Student's t-test (paired), with p=0.05 or less considered significant.

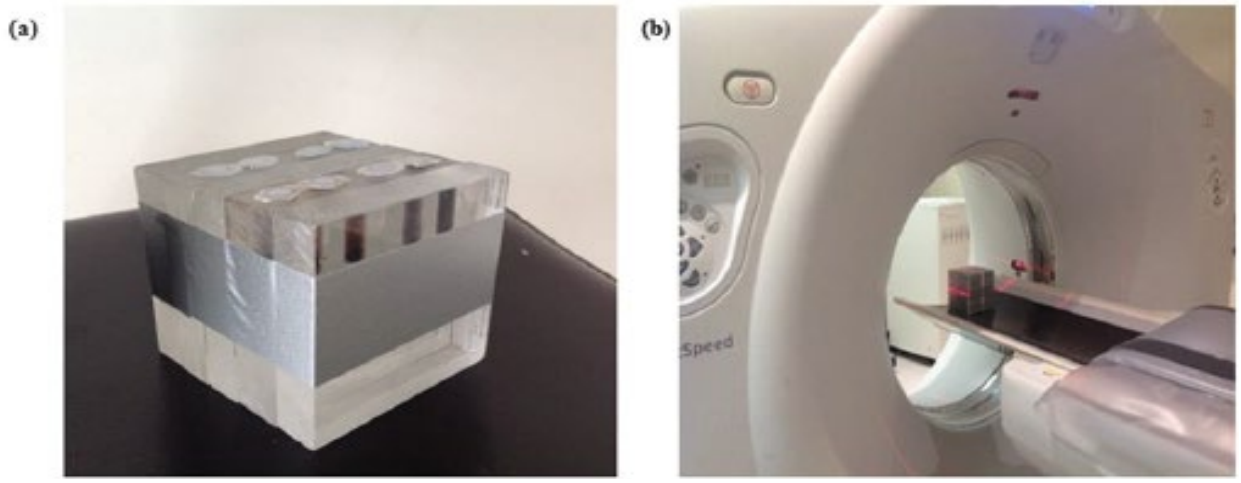

Figure 1: (a) Perspex phantom containing contrast agent solutions, and **(b)** the phantom positioned at the iso-center of the CT gentry.

Results and Discussion

Synthesis and characterization of PVP coated Bi_2S_3 NPs

The PVP-coated Bi_2S_3 NPs were fabricated as previously described using a two-step process, whereby oleic acid coated Bi_2S_3 NPs are initially prepared and then coated with PVP [40]. In this instance, the reaction temperature was reduced to 110°C to facilitate the formation of slightly larger NPs, to obtain the optimal size for CT attenuation. Lower temperatures (<110°C) allow larger metallic nanomaterials to increase in size [37,44]. The optimal NP sizes for CT attenuation have been reported to be between 4 and 20 nm [45]. Previous studies have also demonstrated that the NP size can be controlled through variation of the reaction temperature [46,47].

Dynamic light scattering (DLS) analysis revealed that the hydrodynamic diameter of the NPs ranged from 4 to 18 nm (mean 5.8 nm) (Figure 2). This was also confirmed *via* transmission electron microscopy (TEM), which provided NPs diameters ranging from 5 to 15 nm (Figure 3), and revealed that the NPs had a spherical morphology. X-ray photon spectroscopy (XPS) of the NPs showed two peaks located at 158.5 and 163.5 eV (Figure 4), which can be attributed to the binding energy of Bi 4f 7/2 and Bi 4f 5/2, respectively, whilst a small peak at 161.4 eV corresponded to the binding energy of S2p. The XPS results, as well as the X-ray diffraction (XRD) results (Figure 5) are in good agreement with previous data on Bi_2S_3 NPs 37.

CT scannings

The range of tube potentials selected in this study (80 to 140 kV) represents the range normally used in clinical CT scanners with contrast agents. The X-ray absorption of Bi_2S_3 NPs was compared to the clinical iodinated contrast agent Iohexol at various concentrations and X-ray tube potentials as shown in Figure 6a-d. As expected, CT numbers (report as Hounsfield units (HU)) increased linearly with increasing concentrations of both Bi_2S_3 NPs and the iodinated contrast agent. This was due to the higher atoms density at higher concentrations, which increased the X-ray attenuation value and subsequently increased the HU density during CT imaging. At all tube potentials (80 to 140 KVp), the CT numbers (HU) were greater for Bi_2S_3 NPs than the iodinated contrast agent at the same concentration, indicating higher absorption -ray, but both displayed the same trend with respect to tube potential. This was also observed in CT cross-sectional slices of Bi_2S_3 NPs and iodinated contrast agent solutions at concentrations of 65 mM and increasing tube potentials (Figure 7). The regions that contained Bi_2S_3 NPs had higher attenuation compared to iodine at all tube potentials, indicating enhanced contrast. This was likely related to differences in interaction between X-rays and the two contrast agents. The dominant interaction of X-rays with tissue and water results from Compton scattering (CS) [48,49]. In contrast, for high atomic number (Z) elements, PE would be more significant than for low Z elements as PE depends strongly on a material's atomic number ($\alpha Z3$). Therefore, the CT attenuation of high Z elements (I or Bi) is greater when compared to the attenuation of water (or soft tissue).

The iodine's k-edge (33.2 KeV) occurs just below 80 KVp and the highest attenuation rate for iodine is expected to be at this energy range. The CT attenuation decreases with increasing energy (80 to 140 KVp) due to the reduction of the probability of both PE and CS since these energies are beyond the K-edge value of I. The difference in the attenuation number by Bi atoms compared to water molecules is expected to be larger than iodine and water. This is because the X-ray interaction probability with Bi decreases due to the reduction in PE and CS, whereas in water there is only reduction in CS. However, across all the range of energies the difference in attenuation between Bi and water is larger compared to that of I and water. It follows that the probability of X-ray interaction is highly dependent on physical density (ρm), electron density (ρe) and atomic number (Z). Thus, it is logical that Bi_2S_3 NP displayed much greater attenuation for applications employing tube potentials between 80 to 140 KVp. It was also noted that Bi_2S_3 NPs exhibited stronger attenuation in CT imaging at 80 KVp than at other potentials. However, between 100 and 140 KVp, the attenuation only slightly changed. The cross-sectional CT images from the contrast phantoms also show similar results, where the area containing Bi at 80 kV had a higher attenuation value than at other X-ray tube voltages. This is due to the high probability of interaction with photons (both PE and CS) at 80 KVp, which is lower at potentials from 100 to 140 KVp. The contrast-to-noise ratio (CNR) of Bi_2S_3 NP and iodinated contrast agents was calculated at equivalent concentrations [26,35,50,51] and 65 mM (Figure 8 a-b). The CNR results are directly dependent on the attenuation number of the contrast agents. The value of CNR increases with increasing concentrations of Bi and I within the system, as more atoms are available at higher

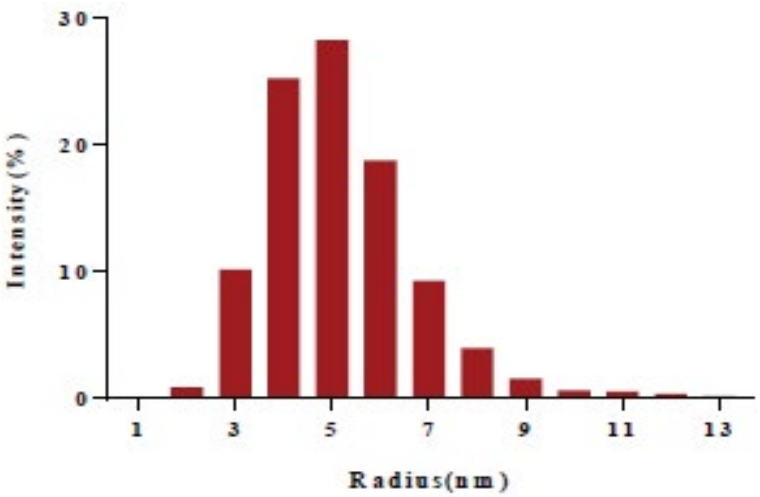

Figure 2: Size distribution of PVP coated Bi2S3 NPs measured by DLS.

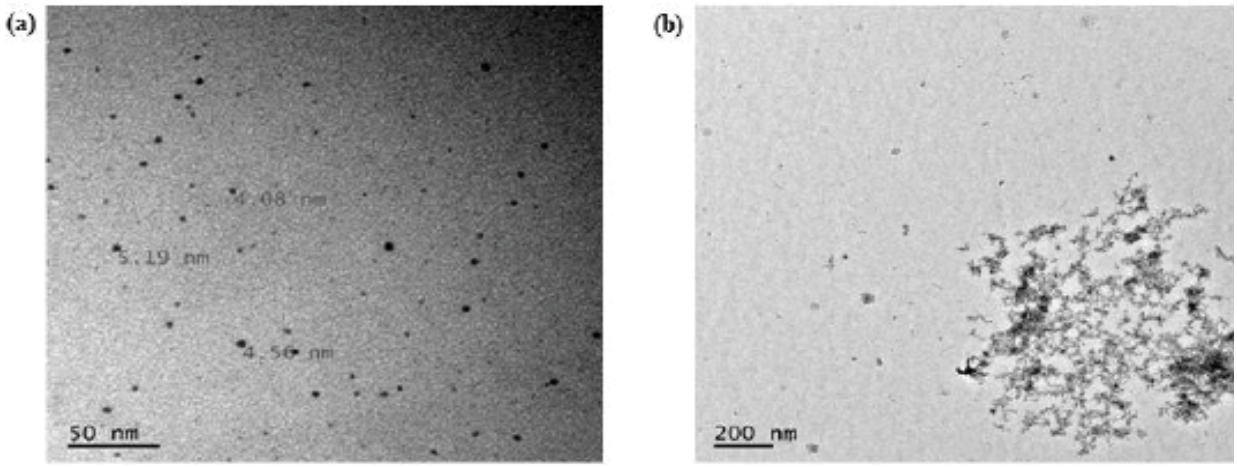

Figure 3: TEM images of PVP coated Bi2S3 NPs showing (a) individual spherical NPs, and (b) aggregates, which may form as a result of the TEM sample preparation.

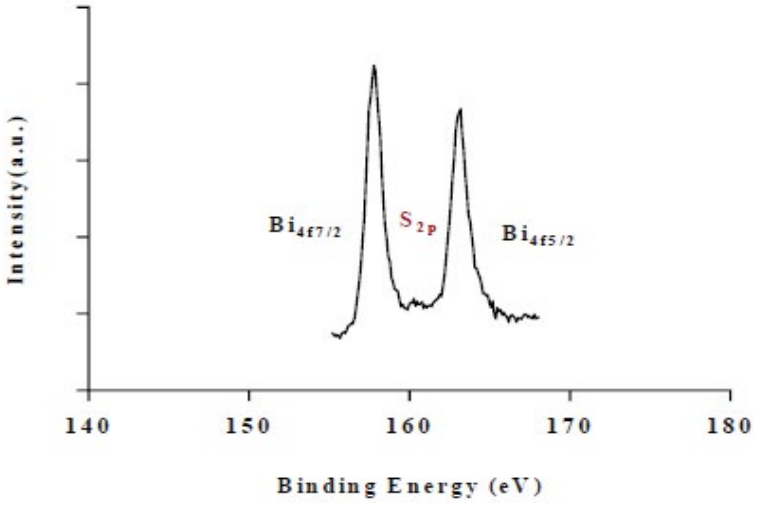

Figure 4: X-ray photon spectra of PVP coated Bi2S3 NPs.

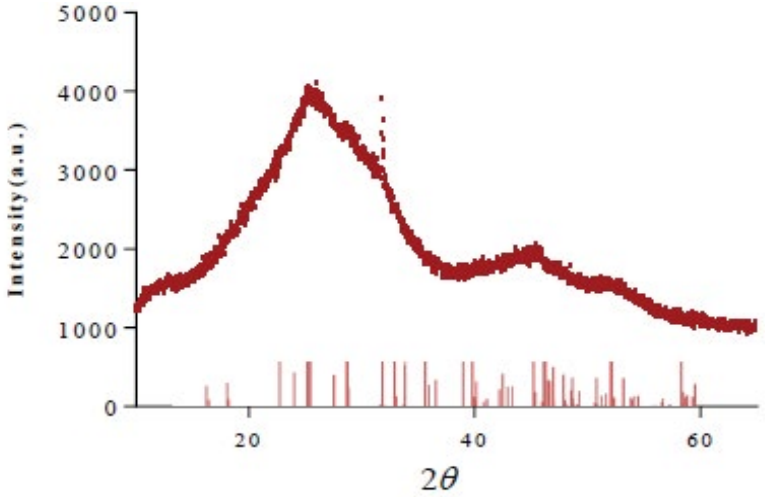

Figure 5: XRD pattern of PVP coated Bi2S3 NPs.

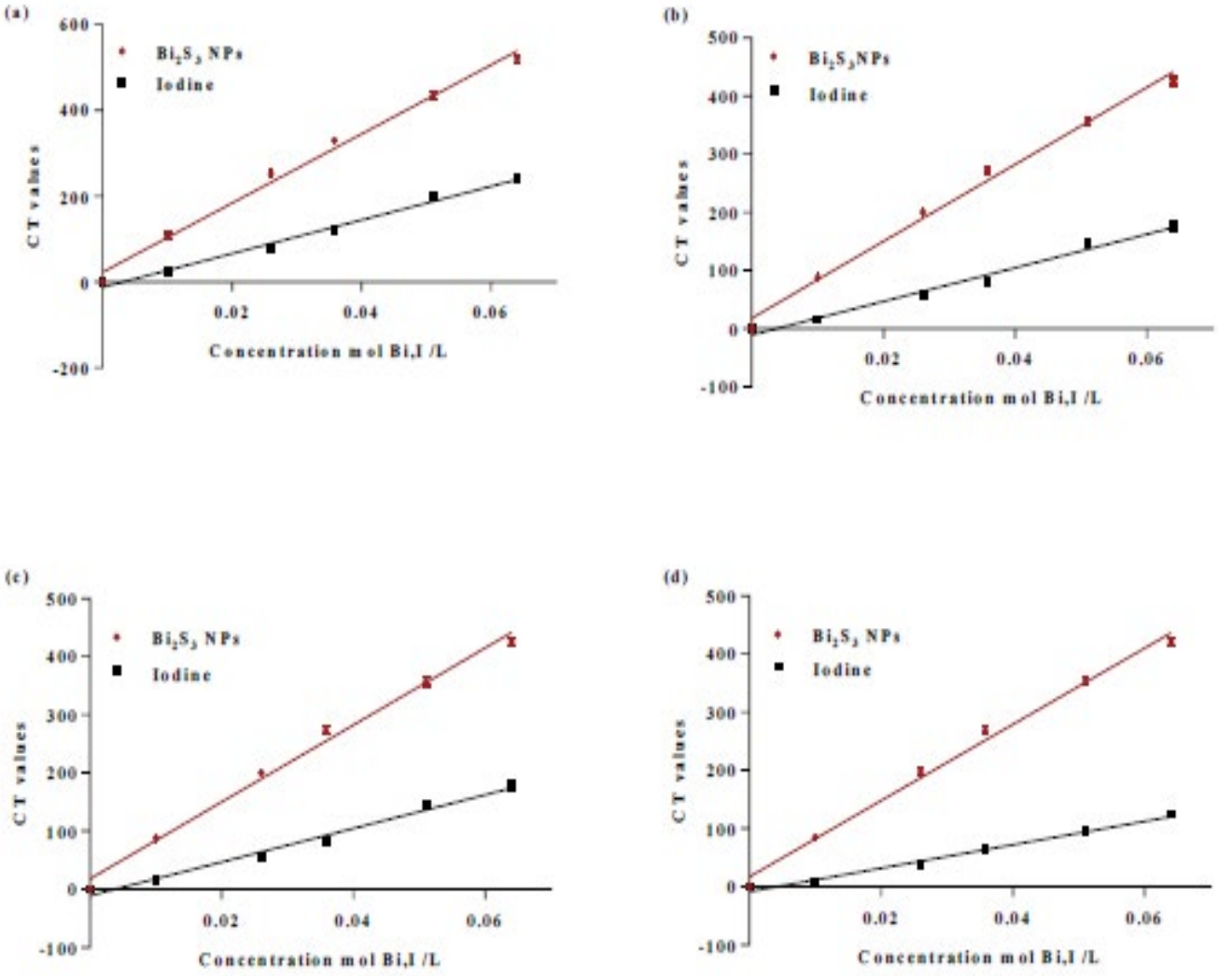

Figure 6: CT numbers for Bi2S3 NPs and the iodinated contrast agent as a function of concentration at tube potentials of (a) 80, (b) 100, (C) 120 and (d) 140 KVp.

concentrations for interaction. Hence, higher attenuation coefficients were obtained leading to bigger differences in attenuation between the solution and the Perspex (container). For the iodinated contrast agent, the CNR was found to decrease with increasing tube potentials at all concentrations. A higher image contrast enhancement for the iodinated contrast agent was observed at a lower tube potential due to the high attenuation value produced from the effect of its k-edge (33.2 KeV) at low energies. The CNR results for the iodinated contrast agent are consistent with previous studies [49,50]. For Bi there was a slight signal reduction from 80 KVp to 140 KVp. The CNR data for Bi NPs follows a similar trend to the iodinated contrast agent. However, at potentials higher than 80 KVp, the Bi NPs CNR showed a pattern of reduction. This could be due to the photon interaction (PE and CS) having a much more pronounced impact at 80 KVp and then decreasing with potentials from 100 to 140 KVp. The effect of the tube potential on contrast enhancement was validated by calculating the differences in CNR values between contrast agents from lower to higher tube potentials at a concentration of 65 mM. Comparison of the CNRs of both contrast agents as a function of tube potentials is represented in Figure 9. At all tube potentials, Bi_2S_3 NP exhibited higher CNR values because of the material's comparatively high atomic number, physical density and electron density. The difference in contrast enhancement between Bi_2S_3 NP and iodinated contrast agents increased with tube potential. At lower KVp, Bi_2S_3 NP showed a one to two-fold increase in contrast enhancement compared to the iodinated contrast agent. This enhancement difference continued to increase and was greatest (three to four times) at 140 KVp. These findings of a 4-fold signal enhancement of Bi_2S_3 NPs over I at 140 KVp are in close agreement to studies by Rabin et al., where a 5-fold increase in attention was reported [12]. Theoretical mass attenuation data were obtained using the NIST mass attenuation plots (Table 1). The mass attenuation coefficient curves of Bi and I were plotted versus photon energy in Figure 10. The total mass attenuation coefficients for both I and Bi are a result of the contribution of both photo-electric and Compton effects. The k-edge value represents an enhancement level threshold in the attenuation of Bi and I at a particular energy. This increased attenuation occurs at 33.2 KeV for I and 91 KeV for Bi, due to the binding energy of the k-shell electrons when the photoelectric absorption occurs. The attenuation data was selected to match the photon energy in KeV and lies between one third and one half of the selected tube potential (80 to 160 KVp). The mass attenuation coefficient decreased for both Bi and I from its highest value at 80 KVp and was reduced at 140 KVp. Interestingly, the attenuation trend for Bi was observed to sharply increase at 160 KVp. The calculated CT numbers followed the same trend as the mass attenuation coefficient. There is close agreement between these results and the calculated theoretical data. The measured mass attenuation coefficient of both agents was strongest at 80 KVp, and as the X-ray tube potential increased, the attenuation decreased. Iodine's K-edge occurs at photon energy of 33.2 KeV, when the tube potential is about 60 KVp and as that potentials increases, the attenuation gradually deceases. At 80 KVp, iodine's attenuative properties are maximized but are not further improved at higher tube potentials. At a high tube potential (>160 KVp), bismuth's k-edge optimum occurs at (91 KeV), where it absorbs a high number of photons. Below this range (80 to 140 KVp), the strongest HU density for Bi occurs at 80 KVp due to the high number of X-ray photons contributing to the PE and CS and once more, less contribution occurs at higher potentials.

The results presented in this study clearly demonstrate the potential for Bi-based NP to act as improved contrast agents at clinically relevant tube potentials when compared to conventional iodinated contrast agents. A lower concentration of Bi NPs can be also be used without resulting in viscosity issues [37]. While it is possible to use higher concentrations of iodinated contrast agents for greater image enhancement, this also increases the risk of adverse reactions in some patients [51]. Taking into consideration these factors, Bi_2S_3 NPs are a promising potential complement contrast agent at the studied tube potentials. This is especially relevant for cases where conventional iodine based contrast media cannot be used due to patient incompatibility (e.g., hypersensitivity reactions). Also importantly, the nanoparticles have a longer circulation time, thus improving their value as targeted agents by maintaining a relatively high blood concentration at the targeted tissue.

Conclusion

This phantom study has shown that the inclusion of Bi NPs provides higher contrast efficacy than iodinated contrast agents at tube potentials of 80 to 140 KVp. These contrast enhancement concen-

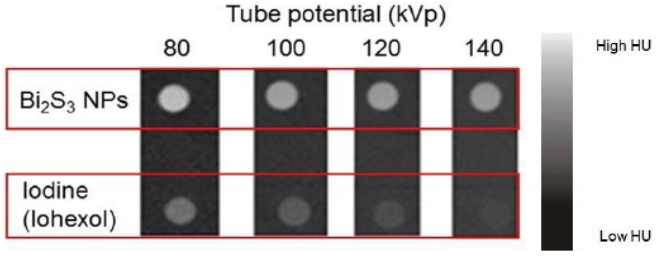

Figure 7: Cross sectional CT images of contrast phantoms containing Bi2S3 NP and iodinated contrast agents. Samples were imaged at equimolar concentrations (65 mM) and tube potentials of 80, 100, 120 and 140 KVp.

Table 1: Mass attenuation coefficients (μ) of measured X-ray energy spectra using published NIST mass attenuation plots. CT valaues for Bi and I were calculated using published NIST mass attenuation data.

KVp	KeV	μBi	μI	μ water	CT # for Bi (×10³)	
80	46	88	14	0.24	364	55
100	60	53	8.0	0.21	247	39
120	67	38	5.6	0.20	186	27
140	80	27	3.3	0.18	149	17
160	91	70	2.5	0.17	411	14

tration increases as it is dependent and also depend on the applied potential to the anode of the x-ray tube, i.e., the average beam energy. At low energy (80 KVp), Bi NPs display a one to two-fold enhancement in attenuation compared to clinical contrast agents. Increasing the tube potential to 140 KVp resulted in even further improved attenuation levels, with Bi NPs displaying 3 to 4-fold greater contrast enhancement over clinical iodinated contrast agents.

This research clearly shows the potential for Bi-based contrast media as an alternative to conventional iodinated contrast agents, particularly in cases where patients have had adverse reactions to conventional iodine-based contrast media and when higher contrast levels are require. As an added advantage, the long vascular half-life of Bi-based contrast agents further improves their value as a replacement to iodine in targeted imaging when prolonged circulation times are necessary.

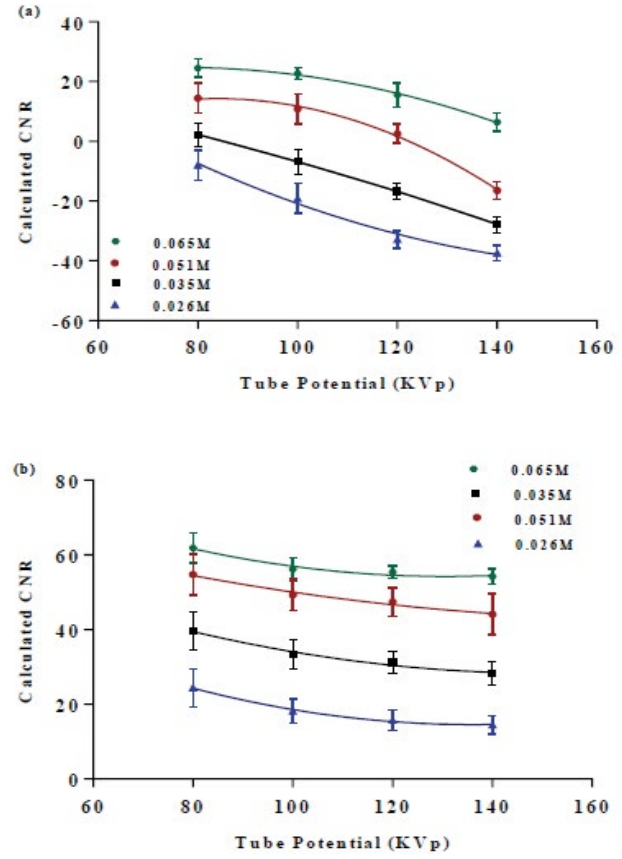

Figure 8: Calculated contrast-to-noise ratios (CNR) for (a) iodinated and (b) Bi2S3 NP contrast agents at different concentrations and tube potentials.

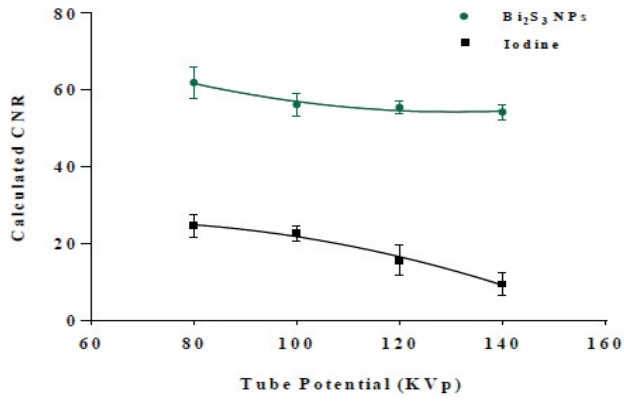

Figure 9: Contrast-to-noise ratios (CNR) obtained from CT images as a function of the tube voltage for Bi2S3 NP and iodinated contrast agents.

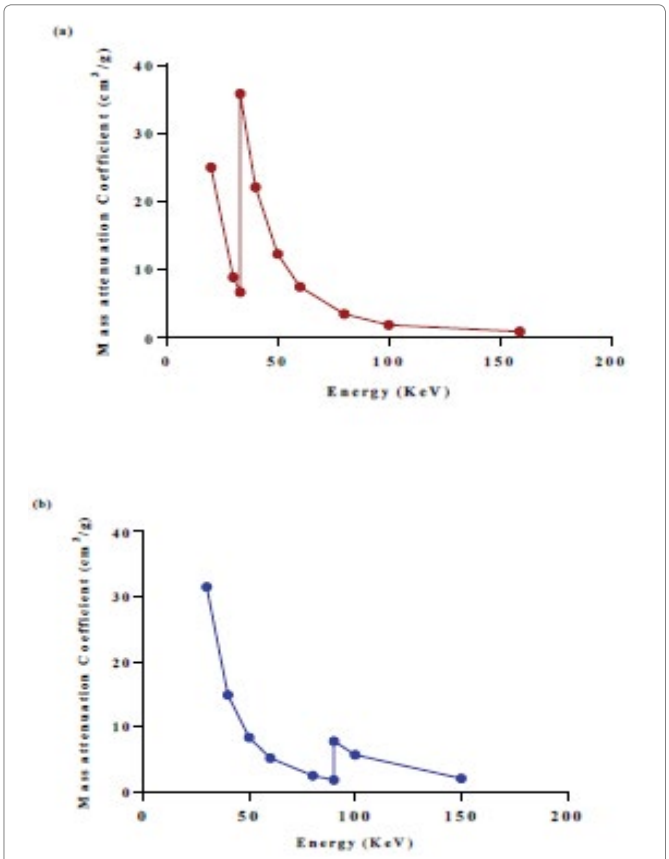

Figure 10: Mass attenuation coefficient as a function of energy showing the K-edge values for (a) iodine and (b) bismuth. Theoretical mass attenuation data were obtained using published NIST mass attenuation plots.

References

1. Doi K (2014) Current status and future potential of computer-aided diagnosis in medical imaging. Br J Radiol 78: s3-s19.
2. Cochard LR (2012) Netter's introduction to imaging. (1st edtn), St. Louis, Mo: Elsevier, St. Louis, Mo.
3. Yu SB, Watson AD (1999) Metal-Based X-ray Contrast Media. Chem Rev 99: 2353-2378.
4. Lee N, Choi SH, Hyeon T (2013) Nano-Sized CT Contrast Agents. Adv Mater 25: 2641-2660.
5. Hyafil F, Cornily JC, Feig JE, Gordon R, Vucic E, et al. (2007) Noninvasive detection of macrophages using a nanoparticulate contrast agent for computed tomography. Nature medicine 13: 636-641.
6. Liu Y, Ai K, Lu L (2012) Nanoparticulate X-ray Computed Tomography Contrast Agents: From Design Validation to in Vivo Applications. Acc Chem Res 45: 1817-1827.
7. Lusic H, Grinstaff MW (2012) X-ray-Computed Tomography Contrast Agents. Chem rev 113: 1641-1666.
8. Jost G, Pietsch H, Lengsfeld P, Hütter J, Sieber MA (2010) The Impact of the Viscosity and Osmolality of Iodine Contrast Agents on Renal Elimination. Invest Radiol 45: 255-261.

9. Singh J, Daftary A (2008) Iodinated contrast media and their adverse reactions. J Nucl Med Technol 36: 69-74.

10. Morcos S, Thomsen H (2001) Adverse reactions to iodinated contrast media. European Radiol 11: 1267-1275.

11. Mattrey RF, Aguirre DA (2003) Advances in contrast media research 1. Acad Radiol 10: 1450-1460.

12. Rabin O, Perez JM, Grimm J, Wojtkiewicz G, Weissleder R (2006) An X-ray computed tomography imaging agent based on long-circulating bismuth sulphide nanoparticles. Nat Mat 5: 118-122.

13. Speck U (2008) Contrast agents: X-ray contrast agents and molecular imaging–a contradiction? In Molecular imaging I, Springer: 167.

14. Hallouard F, Anton N, Choquet P, Constantinesco A, Vandamme T (2010) Iodinated blood pool contrast media for preclinical X-ray imaging applications--a review. Biomaterials 31: 6249-6268.

15. Zukiwski AA, David CL, Coan J, Wallace S, Gutterman JU, et al. Increased incidence of hypersensitivity to iodine-containing radiographic contrast media after interleukin-2 administration. Cancer 65: 1521-1524.

16. Webb JA, Stacul F, Thomsen HS, Morcos SK (2003) Late adverse reactions to intravascular iodinated contrast media. Eur Radiol 13: 181-184.

17. Fleischmann D (2003) Use of high concentration contrast media: principles and rationale-vascular district. Eur J Radiol 45: S88-S93.

18. Krause W, Leike J, Schuhmann-Giampieri G, Sachse A, Schmiedl U, et al. Iopromide-carrying liposomes as a contrast agent for the liver. Acad Radiol 3: S235- S237.

19. Kweon S, Lee HJ, Hyung WJ, Suh J, Lim JS, et al. (2010) Liposomes coloaded with iopamidol/lipiodol as a RES-targeted contrast agent for computed tomography imaging. Pharm Res 27: 1408-1415.

20. Rivera EJ, Tran LA, Hernández-Rivera M, Yoon D, Mikos AG, et al. Bismuth@ US-tubes as a potential contrast agent for X-ray imaging applications. J Mater Chem B 1: 4792-4800.

21. Popovtzer R, Agrawal A, Kotov NA, Popovtzer A, Balter J, et al. (2008) Targeted gold nanoparticles enable molecular CT imaging of cancer. Nano lett 8: 4593-4596.

22. Wyss C, Schaefer SC, Juillerat-Jeanneret L, Lagopoulos L, Lehr HA, et al. (2009) Molecular imaging by micro-CT: specific E-selectin imaging. European radiology 19: 2487-2494.

23. Burda C, Xiaobo C, Narayanan R, El-Sayed MA (2005) Chemistry and Properties of Nanocrystals of Different Shapes. Chem Rev 105: 1025-1102.

24. Cai QY, Kim SH, Choi KS, Kim SY, Byun SJ, et al. (2007) Colloidal gold nanoparticles as a blood-pool contrast agent for X-ray computed tomography in mice. Invest Radiol 42: 797-806.

25. Hainfeld JF, Slatkin DN, Smilowitz HM (2004) The use of gold nanoparticles to enhance radiotherapy in mice. Physics in Medicine and Biology 49: N309.

26. Hainfeld JF, Slatkin DN, Focella TM, Smilowitz HM (2006) Gold nanoparticles: a new X-ray contrast agent. Br J Radiol 79: 248-253.

27. Dykman LA, Khlebtsov N (2011) Gold Nanoparticles in Biology and Medicine: Recent Advances and Prospects. Acta Naturae 3: 34-55.

28. Albanese A, Tang PS, Chan WC (2012) The effect of nanoparticle size, shape, and surface chemistry on biological systems. Annu Rev Biomed Eng 14: 1-16.

29. Briand GG, Burford N (1999) Bismuth compounds and preparations with biological or medicinal relevance. Chem Rev 99: 2601-2658.

30. Larsen A, Martiny N, Stoltenberg M, Danscher G, Rungby J (2003) Gastrointestinal and systemic uptake of bismuth in mice after oral exposure. Pharmacol Toxicol 93: 82-90

31. Tillman L, Drake F, Dixon J, Wood J (1996) Safety of bismuth in the treatment of gastrointestinal diseases. Alimentary Pharmacology & Therapeutics 10: 459-467.

32. Andrews PC, Ferrero RL, Forsyth CM, Junk PC, Maclellan JG, et al. (2011) Bismuth(III) Saccharinate and Thiosaccharinate Complexes and the Effect of Ligand Substitution on Their Activity against Helicobacter pylori. Organometallics 30: 6283-6291.

33. Gisbert JP (2011) Helicobacter pylori eradication: A new, single-capsule bismuth-containing quadruple therapy. Nature Reviews Gastroenterology and Hepatology 8: 307-309.

34. Malfertheiner P, Bazzoli F, Delchier JC, Celiñski K, Giguère M, et al. (2011) Helicobacter pylori eradication with a capsule containing bismuth subcitrate potassium, metronidazole, and tetracycline given with omeprazole versus clarithromycin-based triple therapy: a randomised, open-label, non-inferiority, phase 3 trial. The Lancet 377: 905-913.

35. Rosenblat TL, McDevitt MR, Mulford DA, Pandit-Taskar N, Divgi CR, et al. (2010) Sequential cytarabine and alpha-particle immunotherapy with bismuth-213-lintuzumab (HuM195) for acute myeloid leukemia. Clin Cancer Res 16: 5303-5311.

36. Leussink BT, Baelde HJ, Broekhuizen TM, E Heer, Der Voet GB, et al. Renal epithelial gene expression profile and bismuth-induced resistance against cisplatin nephrotoxicity. Human Exp Toxicol 22: 535-540.

37. Ai K, Liu Y, Liu J, Yuan Q, He Y, et al. (2011) Large-Scale Synthesis of Bi2S3 Nanodots as a Contrast Agent. Advanced Materials 23: 4886-4892.

38. Brown AL, Naha PC, Benavides V, Litt HI, Goforth AM, et al. (2014) Synthesis, X-ray Opacity, and Biological Compatibility of Ultra-High Payload Elemental Bismuth Nanoparticle X-ray Contrast Agents. Chem Mater 26: 2266- 2274.

39. Fang Y, Peng C, Guo R, Zheng L, Qin J, (2013) Dendrimer-stabilized bismuth sulfide nanoparticles: synthesis, characterization, and potential computed tomography imaging applications. Analyst 138: 3172-3180.

40. Algethami M, Geso M, Piva T, Blencowe A, Lu L, et al. (2015) Radiation Dose Enhancement Using Bi2S3 Nanoparticles in Cultured Mouse PC3 Prostate and B16 Melanoma Cells. NanoWorld Journal 1: 97.

41. Kinsella JM, Jimenez RE, Karmali PP, Rush AM, Kotamraju VR, et al. (2011) X-ray computed tomography imaging of breast cancer by using targeted peptide-labeled bismuth sulfide nanoparticles. Angew Chem Int Ed Engl 50: 12308-12311.

42. Alqathami M, Blencowe A, Geso M, G. Ibbott (2016) Quantitative 3D Determination of Radiosensitization by Bismuth-Based Nanoparticles. J Biomed Nanotechnol12: 464471.

43. Funama Y, Awai K, Nakayama Y, Kakei K, Nagasue N, et al. (2005) Radiation dose reduction without degradation of low-contrast detectability at abdominal multisection CT with a low-tube voltage technique: Phantom study. Radiology 237: 905-910.

44. A. Pathak (2013) Aqueous Medium Synthesis Route for Randomly Stacked Molybdenum Disulfide. Journal of Nanoparticles 671214.

45. C Xu, GA Tung, Sun S (2008) Size and Concentration Effect of Gold Nanoparticles on X-ray Attenuation As Measured on Computed Tomography. Chemistry of Materials 20: 4167-4169.

46. Xiliang Q, Yang C, Tiesong L, Peng H, Jun W, et al. (2014) Large-Scale Synthesis of Silver Nanoparticles by Aqueous Reduction for Low-Temperature Sintering Bonding. J Nanomaterials 594873.

47. Burda C, Chen X, Narayanan R, El-Sayed MA (2005) Chemistry and Properties of Nanocrystals of Different Shapes. Chemical reviews 105: 1025-1102.

48. Murakami Y, Kakeda S, Kamada K, Ohnari N, Nishimura J, et al. (2010) Effect of Tube Voltage on Image Quality in 64-Section Multidetector 3D CT Angiography: Evaluation with a Vascular Phantom with Superimposed Bone Skull Structures. American Journal of Neuroradiology 31: 620-625.

49. Razak HRA, Rahmat SMSS, Saad WMM (2013) Effects of different tube potentials and iodine concentrations on image enhancement, contrast-to-noise ratio and noise in micro-CT images: a phantom study. Quantitative imaging in medicine and surgery 3: 256-261.

50. Szucs-Farkas Z, Verdun FR, Allmen G, Mini RL, P Vock (2008) Effect of X-ray Tube Parameters, Iodine Concentration, and Patient Size on Image Quality in Pulmonary Computed Tomography Angiography: A Chest-Phantom-Study. Investigative radiology 43: 374-381.

51. Maddox TG (2002) Adverse reactions to contrast material: Recognition, prevention, and treatment. American family physician 66: 1229-1234.

Author Affiliation

Top

[1]*Discipline of Medical Radiations, School of Health and Biomedical sciences, RMIT University, Melbourne, Victoria 3109, Australia*

[2]*School of Pharmacy and Medical Sciences, University of South Australia, Adelaide, South Australia 5000, Australia*

[3]*Future Industries Institute, University of South Australia, Mawson Lakes, South Australia 5095, Australia*

[4]*Discipline of Biomedical Sciences, School of Health and Biomedical sciences, RMIT University, Melbourne, Victoria 3109, Australia*